Cyclic AMP-induced reversible EPAC1 condensates regulate histone transcription

Liliana Iannucci
Department of Molecular Medicine, University of Pavia
Anna Maria D'Erchia
University of Bari https://orcid.org/0000-0002-4627-0626
Ernesto Picardi
University of Bari https://orcid.org/0000-0002-6549-0114
Daniela Bettio
University of Padua
Francesca Grisan
Foundation for Advanced Biomedical Research, Veneto Institute of Molecular Medicine
Filippo Conca
University of Pavia https://orcid.org/0000-0002-9771-5701
Nicoletta Surdo
National Research Council
Leonardo Salviati
Clinical Genetics Unit, Department of Woman and Child Health, University of Padova,
https://orcid.org/0000-0001-5642-9963
Luciano Milanesi
National Research Council
Graziano Pesole
Bari University https://orcid.org/0000-0003-3663-0859
Konstantinos Lefkimmiatis (konstantinos.lefkimmiatis@unipv.it)
University of Pavia https://orcid.org/0000-0001-7137-7866

Article

Keywords:

Posted Date: July 7th, 2022

DOI: https://doi.org/10.21203/rs.3.rs-1428158/v1

Cyclic AMP-induced reversible EPAC1 condensates regulate histone transcription

Liliana Felicia Iannucci[1,2], Anna Maria D'Erchia[3], Ernesto Picardi[3], Daniela Bettio[4], Francesca Grisan[2], Filippo Conca[1,2], Nicoletta Concetta Surdo[5], Leonardo Salviati[4], Luciano Milanesi[6], Graziano Pesole[3], and Konstantinos Lefkimmiatis[1,2,*].

1. Department of Molecular Medicine, University of Pavia, Pavia, Italy
2. Foundation for Advanced Biomedical Research, Veneto Institute of Molecular Medicine, Padua, Italy
3. Department of Bioscience, Biotechnology, and Biopharmaceutics, University of Bari "Aldo Moro", Bari Italy
4. Clinical Genetics Unit, Department of Women's and Children's Health, University of Padua, Padua, Italy
5. Neuroscience institute, Italian National Research Council, Padua, Italy
6. Institute of Biomedical Technologies, Italian National Research Council, Milan, Italy

* Corresponding author

The second messenger 3',5'-cyclic adenosine monophosphate (cAMP) regulates many nuclear processes including transcription[1], pre-mRNA splicing[2] and mitosis[3]. While most functions are attributed to protein kinase A (PKA)[4,5], accumulating evidence suggests that not all nuclear cAMP-dependent effects are mediated by this kinase[6], implying that other effectors are involved. Here we explore the nuclear roles of Exchange Protein Activated by cAMP 1 (EPAC1). We find that EPAC1 enters the nucleus through the synergy of two aminoacidic domains and there, in response to cAMP, forms reversible biomolecular condensates through liquid-liquid phase separation. This phenomenon depends on intrinsically disordered regions present at its amino-terminus and is independent of PKA. Finally, we demonstrate that nuclear EPAC1 condensates assemble at genomic loci on chromosome 6 and promote the transcription of a histone gene cluster. Collectively, our data reveal an unexpected mechanism through which cAMP contributes to nuclear spatial compartmentalization and promotes the transcription of specific genes.

Based on our current understanding most cAMP-dependent nuclear effects, especially transcription, depend on PKA, a tetrameric cAMP-responsive serine/threonine kinase composed by two regulatory (PKA-Rs) and two catalytic subunits (PKA-Cs)[7,8]. The classic model postulates that, in response to cAMP, extra-nuclear PKA tetramers release their PKA-Cs which can diffuse in the nucleus[9], whilst eventual nuclear PKA tetramers can be activated *in situ*[4,5]. While the obvious interpreter of nuclear cAMP signals seems PKA, its nuclear actions are limited by a number of mechanisms. Nuclear PKA activation is blocked by phosphodiesterase (PDE)-dependent cAMP hydrolysis[5], while nuclear PKA-Cs are contrasted by protein kinase inhibitors (PKIs), a family of proteins that can complex with PKA-Cs and vehicle them to the cytosol[10,11]. In addition to these regulatory mechanisms, we and others recently reported that nuclear PKA-dependent phosphorylation is strongly inhibited by phosphatases in several cell types[11–15]. These findings are in line with a number of studies suggesting that PKA it not the sole responsible for all cAMP-driven nuclear functions, but other cAMP effectors are implicated[6,16–18].

EPAC1 (gene RAPGEF3) has been shown to participate in the regulation of nuclear events, such as the translocation of DNA-protein kinase (DNA-PK)[19] and histone deacetylase 4 (HDAC4)[20] and the PGE2-dependent β-catenin activation[21]. EPAC1 can be found soluble in the cytosol but also at the nuclear envelope complexed with the nuclear pore component RAN Binding Protein 2 (RANBP2)[22]. It is assumed that engaging with RANBP2 is necessary and sufficient for the entry of EPAC1 in the nucleus[23,24], however the mechanism through which effectively enters is not defined. To test this, we performed *in silico* analysis (NLS Mapper)[25] and identified two putative nuclear localization sequences (NLS) within EPAC1 (**Extended Data Fig. 1a**). One of these (amino acids (AAs) 732-764) partially overlapped with the nuclear pore localization sequence previously reported[24], while the other (AAs 179-208) has never been tested. As shown in **Extended Data Fig. 1b**, deletion of each of these regions significantly decreased the nuclear EPAC1 content in HEK293 cells (HEK), independently of its activation status, suggesting that both domains were important for nuclear import. To better understand the role of each sequence, we deleted these regions in an EPAC1 construct that was tagged in its amino-terminus (N-terminus) with YFP (hereafter EPAC1-YFP)[26]. As shown in **Extended Data Fig. 1c left panels** EPAC1$^{\Delta 732\text{-}764}$-YFP lost its nuclear envelope and nuclear localization, as expected[22,24], while EPAC1$^{\Delta 179\text{-}208}$-YFP was unable to enter the nucleus but retained its ability to both, recognize the nuclear envelope (**Extended Data Fig. 1c right panels**) and complex with RANBP2, as shown by immunofluorescence experiments (**Extended Data Fig. 1d**). Taken

together our data clearly suggest that EPAC1 enters the nucleus thanks to a mechanism relying on two distinct regions, AAs 732-764 for engaging the nuclear pore and AAs 179-208 for entering the nucleus.

The identification of a specific mechanism that warrants the entry of EPAC1 in the nucleus is a strong indication for a functional role in this compartment. To test how the nuclear moiety of EPAC1 (nEPAC1) reacts in response to cAMP, we overexpressed EPAC1-YFP in EPAC1-deficient HEK cells **Fig. 1a**. As shown in **Fig. 1b** & **Extended Data Movie 1**, in untreated cells EPAC1-YFP localized in the cytosol, nuclear envelope and nucleus. In response to intracellular cAMP elevation, cytosolic EPAC1-YFP rapidly moved to the plasma membrane, as expected[7]. On the other hand, nuclear EPAC1-YFP oligomerized in well-defined spherical structures in approximately 40% of the EPAC1-YFP expressing cells (**Fig. 1c**). These structures did not depend on the fluorophore, since both an untagged and a carboxy-terminus mCherry2-tagged EPAC1 (mCherry2-EPAC1) formed similar puncta in the nucleus of HEK cells in response to cAMP (**Extended Data Fig. 2a,b**). Importantly, the generation of nEPAC1 oligomers was independent of PKA activity since the PKA inhibitor H89 was unable to block their insurgence (**Extended Data Fig. 2c second panel**) while, in addition, the EPAC-specific cell permeant cAMP analog 8-pCPT-2'-O-Me-cAMP-AM (8CPT-cAMP) induced the formation of EPAC1-YFP puncta (**Extended Data Fig. 2c third panel**). Nuclear EPAC1 oligomers were also formed when cells were challenged with norepinephrine which produced a much smaller cAMP increase (roughly 50% of FSK/IBMX), as measured by a FRET-based cAMP sensitive sensor[2] (**Extended Data Fig. 2d**). In response to cAMP binding, EPAC1 exits its autoinhibited state assumes an active conformation and activates the small GTPases Rap1 and Rap2[27,28]. To test whether Rap1&2 activation is important for nuclear oligomer formation we used a catalytically dead mutant (EPAC1$^{TF781\text{-}782AA}$-YFP)[29] and found that was able to oligomerize in response to cAMP suggesting against the involvement of these proteins (**Extended Data Fig. 2e**). Thus, we conclude that upon cAMP elevation, EPAC1 forms nuclear puncta/oligomers.

To test whether this behavior was recapitulated by endogenous EPAC1, we used two different cell models, Human Umbilical Vein Endothelial Cells (HUVEC) and an ovary adenocarcinoma cell line (SKOV3) both expressing EPAC1 in the nucleus as confirmed by nuclear fractionation and Western Blotting (**Fig. 1d**). In cells treated with DMSO (vehicle control), endogenous EPAC1 appeared mostly soluble with a small number of oligomers. Nuclear EPAC1 oligomerization was drastically enhanced

when intracellular cAMP levels were increased by treating cells for 30 to 40 minutes with forskolin (FSK) a broad activator of transmembrane adenylyl cyclases combined to 3-isobutyl-1-methylxanthine (IBMX) to inhibit PDEs (**Fig. 1e**). We also noted that this treatment had different effects on the cytosolic EPAC1 which moved to plasma membrane or mitochondria depending on the cell type[6]. In line with these observations, a cAMP binding-deficient EPAC1 (EPAC1^{R279E}-YFP)[26] was unable to form oligomers (**Fig. 1f**) demonstrating that cAMP is necessary and sufficient to trigger nEPAC1 oligomerization. Collectively these data suggest that nEPAC1 oligomers could represent a novel signalling modality through which cAMP signals are interpreted in the nucleus. However, to be considered a signalling event, nEPAC1 oligomers should be reversible and reproducible in response to cAMP. As shown in **Fig. 1g** and **Extended Data Movie 2** EPAC1-YFP puncta were mostly nuclear and rapidly dissipated after rinsing the cAMP-generating agonists and rapidly reformed in the next round of stimulation, substantially mirroring the behavior of a signalling event.

The dynamic nature of nEPAC1 oligomers together with their characteristic spherical shape (**Fig. 2a**) suggested that these structures could be biomolecular condensates or membraneless organelles[30]. Biomolecular condensates are thought to generate through weak, multivalent, and dynamic interactions among proteins and/or nucleic acids in the absence of a bounding membrane[30,31]. To verify the nature of nEPAC1-based oligomers we thus tested several defining indicators of condensates[32]. As shown in **Fig. 2b** & **Extended Data Movie 3**, nEPAC1-YFP oligomers were rapidly dissolved when 1,6-hexaenadiol, an aliphatic alcohol that interferes with weak hydrophobic interactions[33] was added in the FSK-IBMX-complemented solution. These data suggested that nEPAC1 condensates through the process of Liquid-Liquid Phase Separation (LLPS). Nuclear EPAC1 oligomers could also undergo fusion events, another indicator of membraneless organelles[32], further substantiating the dynamic liquid-like nature of these structures (**Fig. 2c** & **Extended Data Movie 4**). Finally, Fluorescence Recovery After Photobleaching (FRAP) experiments (**Fig. 2d** & **Extended Data Movie 5)** demonstrated that nEPAC1-YFP condensates rapidly recovered (quantified in **Fig. 2e**) after laser-induced bleaching, further indicating that nEPAC1 condensates are formed by LLPS.

Next, we tested EPAC1 for the presence of intrinsically disordered regions (IDRs), which represent a cardinal characteristic of proteins able to undergo LLPS[34]. As shown in **Fig. 3a** *in silico* analysis using

the algorithm (D^2p^2)[35] identified several IDRs within EPAC1, especially within its catalytic (C-terminus) and regulatory (N-terminus). We first tested the latter and found that a deletion mutant of EPAC1 lacking the first 148 AAs (EPAC1$^{\Delta 2\text{-}148}$-YFP), was unable to form condensates in response to cAMP elevations even though it retains intact its ability to bind to cAMP and undergo conformational changes[29] (**Fig. 3b**). To better define the precise sub-domains responsible for nEPAC1 condensate formation we generated several other mutants. Interestingly, deletion of AAs 2-24 (EPAC1$^{\Delta 2\text{-}24}$-YFP) abolished the ability of nEPAC1 to generate condensates (**Fig. 3c)** as did the deletion of a region containing the DEP domain (AAs 48-148) EPAC1$^{\Delta 48\text{-}148}$-YFP (**Fig. 3d)**. We also noted that the plasma membrane localization of these mutants was impeded, however this was expected since the N-terminus is responsible for EPAC1 membrane localization[6]. On the contrary, the ability to generate condensates of mutants lacking intermediate AAs, EPAC1$^{\Delta 25\text{-}50}$-YFP and EPAC1$^{\Delta 51\text{-}73}$-YFP was unaffected (**Extended Data Fig. 3a,b)**. In addition to the two domains (AAs 2-24 and 74-148) that proved to be necessary for the nEPAC1 condensates, we also identified an aminoacidic region (AAs 145-175) that appears to be crucial for the cAMP-dependent regulation of this phenomenon. In fact, as shown in **Fig. 3e**, a deletion mutant lacking this region (EPAC1$^{\Delta 145\text{-}175}$-YFP) constitutively forms condensates independently of the presence of cAMP. Taken together, these data indicate that both the formation of EPAC1 membraneless organelles and their cAMP dependence are regulated by specific regions within the EPAC1 N-terminus.

In recent years nuclear membraneless organelles emerged as central regulators of a plethora of nuclear processes, from transcription to RNA processing to chromosome structure and maintainance[30]. While several types of nuclear multiprotein condensates have been described[30,36], the precise composition of many remains elusive. Since we demonstrated that nEPAC1 is a condensation-proficient protein, we next tested whether it participated in other already known nuclear membraneless organelles. As shown in **Fig. 4a**, nEPAC1-YFP was not present either in the nucleoli or in cajal bodies as demonstrated by immunofluorescence using their respective markers nucleolin[37] and Survival Motor Neuron protein (SMN)[38]. On the contrary, as shown in **Fig. 4b**, nEPAC1 condensates overlapped at least in part with promyelocytic leukemia protein (PML)-based nuclear bodies (PML-NBs) and the Nuclear Protein of the ATM Locus (NPAT), a marker of Histone Locus Bodies (HLBs)[38] (**Fig. 4c**). These data suggested that nEPAC1 may be a component of hybrid condensates. However, its structural importance in both HLBs and PML-NBs seems of lesser importance since both types of these condensates were present in unstimulated HEK cells where

nuclear EPAC1-YFP is diffused throughout the nucleoplasm (DMSO treatment **Fig. 4c**). These considerations raised the possibility that nEPAC1 may exert a functional or a regulatory role on other nuclear bodies.

A primary function of nuclear membraneless organelles is to regulate transcription. For instance, HLBs contain factors required for processing histone pre-mRNAs[38], while PML-NBs have been found to associate with transcriptionally active sites[39]. To test the involvement of nEPAC1 condensates in transcriptional regulation we used high throughput whole transcriptome RNA-sequencing. As illustrated in **Fig. 5a,** EPAC1-deficient HEK cells were transfected with EPAC1-YFP or, as control, the EPAC1$^{\Delta 2\text{-}148}$-YFP mutant which is unable to phase separate (**Fig. 3b**). Twenty-four hours after transfection, cells were treated with the cell permeant EPAC-selective cAMP analog 8CPT-cAMP (5µM) to induce condensate formation, or with DMSO (vehicle) as control for 40 minutes. We strategically choose 8CPT-cAMP in order to avoid PKA-dependent transcription events, while the 40 min timepoint was chosen since the cAMP effects on transcription peak between 30 and 60 minutes[1]. After treatment, EPAC1-expressing cells were Fluorescence-Activated Cell Sorting (FACS)-sorted using the YFP fluorescence and total RNA was extracted. Directional RNA sequencing of rRNA-depleted total RNA generated an average of ~76 million reads per sample, of which 64% to 75% could be aligned to the reference genome, suggesting very good coverage and sequencing depth with low ribosomal RNA contamination. RNA-seq data analysis identified 21,705 annotated genes as expressed in at least one of the sequenced samples. Principal Component Analysis (PCA) indicated anomalous behavior for one of the three biological replicates of the EPAC1-YFP treated with 8CPT-cAMP sample, which was not included to further analyses. We used CufDif2[40] for the identification of differentially expressed genes in all samples (p-value ≤ 0.01). When compared to untransfected cells, overexpression of EPAC1-YFP affected the transcription of 662 genes while overexpression of EPAC1$^{\Delta 2\text{-}148}$-YFP impinged on the expression of 1803 genes (**Extended Data Fig. 4a,b**). The expression levels of the two constructs were virtually identical as indicated by the fold increase compared to the untransfected cells calculated in the RNAseq experiments (log_2Fold 12.89 for EPAC1-YFP and 12.74 for EPAC1$^{\Delta 2\text{-}148}$-YFP). As shown in **Fig. 5b**, 40 min treatment of EPAC1-YFP-expressing cells with 8CPT-cAMP-induced modest but significant changes in the expression of 166 genes while the same treatment affected the expression of 42 genes when EPAC1$^{\Delta 2\text{-}148}$-YFP was expressed (**Fig. 5c**). The effect of 8CPT-cAMP in the transcriptional signature of untransfected HEK cells was negligible (**Extended Data Fig. 4c**), further confirming the absence of EPAC1 in HEK and,

most importantly, suggesting that the differences between the effects of the two constructs depended exclusively on their ability to form or not nuclear condensates. When we compared the two sets of genes regulated by 8CPT-cAMP treatment in EPAC1-YFP and EPAC1$^{\Delta 2\text{-}148}$-YFP we found no overlap (only one gene was in common). Interestingly, further analysis revealed that upon activation, EPAC1-YFP but not EPAC1$^{\Delta 2\text{-}148}$-YFP, affected the transcription of 77 nuclear proteins, among which 28 (36%) were histones (**Fig. 5b inset**) the vast majority of which (20/28) (71%) located to the large cluster of histone genes on human chromosome 6 (6p21–p22), which represented 16.9% of the differentially expressed genes (DEGs) (**Fig. 5d**). In line with this observation, histone genes were differentially expressed only in response to EPAC1-YFP overexpression (13/662 DEGs) as compared to naive HEK cells. While, on the other hand, overexpression of the EPAC1$^{\Delta 2\text{-}148}$-YFP had a negligible effect on histone expression (3/1803 DEGs). The strikingly high incidence of histones in our RNAseq analysis together with our previous observation that EPAC1-YFP condensates colocalized with the HLBs-marker NPAT (**Fig. 4b**), strongly suggested that the activation of the nuclear moiety of EPAC1 is a regulatory event of HLBs activity. Histones are organized in gene clusters and their transcription depends on several factors that are enriched in HLBs[38]. To determine whether nEPAC1 is directly involved in the regulation of histone transcription we designed a custom fluorescent probe for the large histone cluster 1 on Chromosome 6p22.2 (design region: chr6:26019341-26201862) and performed fluorescence colocalization experiments between EPAC1-YFP condensates and the Chromosome 6p22.2 region visualized by fluorescence *in situ* hybridization (FISH), in cells treated with FSK-IBMX (to increase cAMP levels) for 40 minutes. As shown in **Fig. 5e**, EPAC1-YFP-based condensates displayed a high degree of colocalization with the Chr6p22.2 probe (overlapping coefficient 0.52), while no colocalization was observed between condensates and an unrelated region (no EPAC1-dependent DEGs present) of the chromosome 21 (21q22.13-q22.2) (overlapping coefficient 0.004) (**Fig.5f**). Taken together our RNA-seq and fluorescence colocalization FISH experiments demonstrate that in response to cAMP elevations, the nuclear moiety of EPAC1 generates condensates in the proximity of the Histone Cluster 1 locus to regulate its transcription.

Nuclear membraneless organelles offer the appropriate three-dimensional organization and components necessary for guaranteeing precise and topologically restricted nuclear functions[30]. These structures gem in response to specific stimuli thanks to highly dynamic processes, however, the mechanisms through which the triggering signal is coupled to the condensate formation remain

elusive. Here, we demonstrate that phase separation of nuclear EPAC1 can be considered a *bona fide* signalling event, controlled by the levels of the second messenger cAMP and impinging on transcription, and possibly on the function of other nuclear condensates. We find that cAMP-triggered nEPAC1 condensates colocalize with NPAT, a marker of histone locus bodies[41] and regulate the expression of a specific histone gene cluster at chromosome 6. To control transcription, nEPAC1-condensates could provide a controlled modality for localizing to the active site important factors in a spatial and temporal manner. Considering the importance of histone levels to cellular proliferation, the nuclear cAMP/EPAC1-condensate axis represents a novel molecular mechanism that could impinge on physiological or pathological cell division. Typically, increases in cAMP levels result in the increased enzymatic activities of its effector proteins. Our findings add a new level of complexity to this cascade as they show that in the case of the nuclear moiety of EPAC1, cAMP elevations result in the generation of hollow compartments that offer a privileged, and transient space where distinct components may be stored, or specific reactions may occur. Based on our findings, it is tempting to speculate that the nuclear moiety of EPAC1 provides the means through which cAMP controls the spatial compartmentalization of the nucleus.

Materials and methods

Reagents

Forskolin (FSK), H-89 dihydrocloride (H89), 3-isobutyl-1-methylxantine (IBMX), dimethyl sulfoxide (DMSO), 1,6-Hexanediol, Phosphate Buffered Saline (PBS), Tween 20, Bovine Serum Albumin (BSA) and Skim Milk Powder were from (Merck KGaA, Darmstadt, Germany). 8- (4- Chlorophenylthio)- 2'-O- methyladenosine- 3', 5'- cyclic monophosphate, acetoxymethyl ester (8-pCPT-2'-O-Me-cAMP-AM) was from BioLog (Biolog Life Science Institute GmbH & Co. KG, Bremen, Germany).

Cell culture and transfection

HEK293 cells were grown in Dulbecco's modified Eagle's high glucose medium (DMEM, ECM0728 Euroclone, Milan, Italy), supplemented with 1% penicillin–streptomycin (Life Technologies, 15140163), and 10% Fetal Bovine Serum (FBS) (Euroclone, Milan, Italy ECS0180). Ovarian adenocarcinoma SK-OV-3 cells were purchased from ATCC and grown in RPMI (Sigma-Aldrich R8758) supplemented with 1% penicillin–streptomycin (Life Technologies, 15140163), and 10% Fetal Bovine Serum (Euroclone, Milan, Italy ECS0180L). Human Umbilical Vein Endothelial Cells (HUVEC) were a gift from the laboratory of Prof. Luca Scorrano (University of Padua). All cell lines

were grown in a humidified incubator at 37 °C and 5% CO_2 atmosphere and tested for mycoplasma contamination every three months. Cells were split when 80-90% confluence was reached, every 2-3 days. For confocal imaging, cells were grown on glass coverslips, coated with poly-L-Lysine (Sigma Aldrich, P4707). Twenty-four hours after plating cells were transfected with Lipofectamine 2000 Reagent (Thermo Fisher Scientific, Waltham, MA, USA) according to the manufacturer's instructions.

In silico Nuclear Localization Sequence (NLS) and disorder enrichment analysis

The EPAC1 aminoacidic sequence was submitted in the NLS Mapper algorithm[25]. Two putative NLS sequences were identified and further analyzed by mutagenesis. The algorithm (D^2P^2)[35] was used to assay disorder propensity for each aminoacid of EPAC1. Putative Intrinsically Disorder Regions (IDRs) scored positively in multiple of the algorithms employed by the D2P2. IDRs that were within functional regions of EPAC1 (cAMP binding domain or Catalytic domain) were not further analyzed. IDRs at the amino terminus were further pursued by mutagenesis.

Plasmids and Mutagenesis

pEGFP-N3-EPAC1 and pEGFP-N3-EPAC1$^{D2\text{-}148}$ were a gift from Prof. Xiaodong Cheng (University of Texas Health Science Center at Houston). EPAC1 subcloning in the vector mCherry2-C1, as well as EPAC1 mutagenesis, were performed using the Takara In-Fusion® HD Cloning kit (638910) according to the manufacturer's instructions. mCherry2-C1 was a gift from Michael Davidson (Addgene plasmid #54563; https://www.addgene.org/54563/).

Cytosol-Nuclei cell fractionation

Cells plated into 10 cm petri dishes and confluent 80-90% were collected and incubated for 10 min on ice in hypotonic buffer (20mM Tris-HCl (pH 7.4), 10 mM KCl, 2 mM MgCl2, 1 mM EGTA, 0.5 mM DTT, 0.3% NP-40), followed by centrifugation at 1000 rcf at 4°C for 5 min to separate the nuclei (pellet) and cytoplasm (supernatant). The pellet was washed twice with isotonic buffer (20 mM Tris-HCl (pH 7.4), 150 mM KCl, 2 mM MgCl2, 1 mM EGTA, 0.5 mM DTT) and then resuspended and incubated in cold RIPA buffer (5 mM Tris-HCl (pH 7.4), 150 mM NaCl, 0.1% SDS, 0.5% sodium deoxycholate, 1% NP-40) and incubated for 10 min on ice. Samples were then centrifuged at 2000 rcf (4°C) for 3 min and supernatant was collected as nucleic lysate. All buffers were supplemented with cOmplete™ Protease Inhibitor Cocktail (Roche Diagnostics) and PhosSTOP™ phosphatase inhibitor cocktail (Roche Diagnostics).

Western Blotting

Cells were lysed in cold RIPA buffer supplemented with protease and phosphatase inhibitors. Lysates (20–30 µg of the single fractions) were loaded onto 4–12% precast polyacrylamide gel (Bolt 4-12%, Bis-Tris plus gels; Thermo Fisher Scientific) for electrophoresis and run at 100V. Proteins were then transferred onto polyvinylidene fluoride (PVDF) membranes (Thermo Fisher Scientific). And blocked for 1 h at room temperature in 10% (w/v) non-fat-dry milk- Tris-buffered saline/Tween 20 (TBST). The membranes were then incubated overnight at 4 °C with continuous rotation with 1:1000 primary antibody in 5% normal milk-TBST. Membranes were washed three times with TBST at room temperature and incubated for 1 h at room temperature with 1:5000 peroxidase-conjugated secondary antibodies. Membranes were developed with enhanced chemiluminescence (Luminata Crescendo Western HRP, Merck Millipore) and imaged using an ImageQuant LAS 4000 mini system equipped with a CCD camera (GE Healthcare, USA). Antibodies used: Anti-GAPDH (Santa Cruz Biotechnology, sc-166574) and anti-Lamin A/C (Sigma, SAB4200236) EPAC1 (Cell Signalling Technologies 4155). For subsequent detections, membranes were stripped using Restore Western Blot Stripping Buffer (Thermo Fisher Scientific, 46430) for 15 min at room temperature and then washed with TBST.

Confocal Live-cell imaging

Cells were plated on 15mm glass coverslips coated with poly-L-Lysine (Sigma Aldrich, P4707). Before imaging experiments, cells were rinsed twice with Ringer's modified buffer (NaCl 125 mM; KCl 5 mM; Na_3PO_4 1 mM; $MgSO_4$ 1 mM; Hepes 20 mM; glucose 5.5 mM; $CaCl_2$ 1 mM; pH adjusted to 7.4 using 1 M NaOH) and mounted onto an open perfusion chamber RC-25F (Warner Instruments, Hamden, CT, USA). Indicated treatments were performed both acutely on stage or cells were pre-treated. Images were collected on a Leica SP5 Confocal scanning microscope using oil immersion 40x (HCX PL Apo lambda blue 40x/1.25 Oil UV, Leica, Wetzlar, Germany) or 60x (HCX PL Apo lambda blue 63x/1.40 Oil UV, Leica, Wetzlar, Germany) objectives and post-processed using FIJI.

FRET

HEK293 cells were plated onto glass coverslips and transfected with the FRET-based cAMP sensor $EPAC^{H187}$. Twenty-four hours after transfection cells were mounted onto an open perfusion chamber RC-25F (Warner Instruments, Hamden, CT, USA) and perfused using a homemade gravity-fed perfusion system. The cells were bathed in Ringer's modified buffer (NaCl 125 mM; KCl 5 mM;

Na_3PO_4 1 mM; $MgSO_4$ 1 mM; Hepes 20 mM; glucose 5.5 mM; $CaCl_2$ 1 mM; pH adjusted to 7.4 using 1 M NaOH). The experiments were performed on an Olympus IX81 inverted microscope (Olympus, Tokyo, Japan) equipped with a beam-splitter (Dual-ViewTM, Optical Insights, Santa Fe, New Mexico, NM, USA) and a CCD camera (F-ViewII, Soft Imaging System, Münster, Germany). The cyan fluorescent protein (mTurquoise) was excited for 200 milliseconds at 430 nm, while the emission fluorescence was collected every 10–15 s for both donor and acceptor fluorophores at 480 and 545 nm, respectively. Automatic image collection and preliminary analysis were performed using the Cell R software (Olympus, Tokyo, Japan) and then analyzed with ImageJ plugin. Raw data were transferred to Excel (Microsoft, Redmond, WA, USA) for background subtraction and generation of the ratios.

Fluorescence Recovery after Photo-Bleaching (FRAP).

HEK293 cells were plated onto glass coverslips and transfected with EPAC1-YFP. Twenty-four hours after transfection cells were mounted onto an open perfusion chamber RC-25F (Warner Instruments, Hamden, CT, USA) and bathed in Ringer's modified buffer (NaCl 125 mM; KCl 5 mM; Na_3PO_4 1 mM; $MgSO_4$ 1 mM; Hepes 20 mM; glucose 5.5 mM; $CaCl_2$ 1 mM; pH adjusted to 7.4 using 1 M NaOH). FRAP experiments were performed on a Leica SP5 Confocal microscope using a 488-nm laser. Bleaching was performed using 100% laser power for 4 cycles, and images were collected every 200-300 ms. Fluorescence intensity at the bleached spot and of the whole cell was measured using the FIJI plugin FRAP Profiler. Values are reported relative to the whole cell to control for photobleaching during acquisition.

DNA Fluorescence in situ hybridization (FISH)

Cells were plated onto glass coverslips and transfected with EPAC1-YFP. After 24 hours cells were fixed with 4% PFA in PBS for 10 min and washed 3 times with PBS. Cells were dehydrated by serial incubations in ethanol 70%, 85% and 100% for 1 min at room temperature. Probe hybridization mixture was prepared by mixing 7 µl of FISH Hybridization Buffer (Agilent G9400A), 1 µl of FISH probe (see below) and 2 µl of water. Five microliters of the mixture were added on a slide and the coverslip was placed on top. Coverslips were sealed with rubber cement. Denaturation was performed at 78 °C for 15 min and slides were incubated at 37 °C in the dark overnight. The coverslip was then incubated in pre-warmed wash buffer 1 (0,4X SSC; 0,3% NP40 pH 7.5) at 73 °C for 2 min, and in wash buffer 2 (2X SSC; 0,1% NP40 pH7) for 1 min at room temperature. Coverslips were air-

dried, mounted on slides using Vectashield (Vector Laboratories), and sealed with nail polish. Images were acquired on a Zeiss LSM900 with Airyscan confocal microscope in modality super-resolution with a 63× objective and processed using FIJI. A specific DNA FISH probe for chromosome 6p22.2 was custom-designed and generated by Agilent to target Histone locus 1. The design input region was chr6:26019490-26201715 (182.226 kb) and the design region was chr6:26019341-26201862 (182.522 kb). While for the control experiments, we used a commercial DNA FISH probe for chromosome 21 (Vysis LSI21 08L54-020) approximately 220 kb with a cytogenetic location of 21q22.13-q22.2 (chr21: 39439949-39659711).

Immunofluorescensce

Cells were then plated on coverslips were coated with poly-L-Lysine (Sigma Aldrich, P4707) and transfected with EPAC1-YFP or its mutant versions. Twenty-four hours after transfection cells were fixed using 4% paraformaldehyde (PFA) (Santa Cruz Biotechnology, sc-281692) in PBS for 10 min. After washing cells 3 times in PBS, the coverslips were put into a humidifying chamber for subsequent steps. Cell permeabilization was performed using 0.2% Triton X100 (Serva, 39795.02) in PBS for 10 min, followed by 3 PBS washes. After blocking with 2% BSA for 1 h cells were incubated with the indicated primary antibodies at a concentration of 1:300 in PBS except for endogenous EPAC1 that was used 1:50). The antibodies used for immunofluorescence were SMN (Santa Cruz Biotechnology, sc-365909); Nucleolin (Sigma, N2662-25UL); NPAT (Santa Cruz Biotechnology, sc-136007); PML (Sigma, PLA-0172); EPAC1-488 (Abcam, ab201506).

RNA sequencing

HEK293 cells were seeded on 10cm petri dishes and transfected with either EPAC1-YFP or its mutant version EPAC1$^{\Delta 2\text{-}148}$-YFP. After 24h cells were treated with DMSO (vehicle control) or 8-pCPT-2'-O-Me-cAMP-AM (5µM) for 40 min. Cells were then FACS-sorted (FACS facility Veneto Institute of Molecular Medicine, Padua, Italy) using the YFP fluorescence. Total RNA was extracted using RNeasy Mini Kit (Qiagen ID: 74104) complemented with on-column DNAse digestion with the RNAse-free DNAse set (Qiagen ID: 79254) according to the manufacturer's instructions. RNA was quantitatively and qualitatively evaluated using NanoDrop 2000c (Thermo Fisher Scientific) and Agilent Bioanalyzer 2100 (Agilent Tecnologies), respectively.

RNA-seq libraries were prepared from 1 µg of total RNA, using the Illumina's TruSeq Stranded Total RNA Sample Preparation Kit (Illumina, San Diego, CA, USA), according to the manufacturer's

protocol. cDNA libraries were qualitatively checked on the Bioanalyzer 2100 and quantified by fluorimetry using the Quant-iTTM PicoGreen® dsDNA Assay Kit (Thermo Fisher Scientific) on NanoDrop™ 3300 Fluorospectrometer (Thermo Fisher Scientific). Sequencing was performed on NextSeq500 platform, generating for each sample almost 100M of 100bp paired-end reads.

Raw RNAseq reads were initially inspected by FASTQC (https://www.bioinformatics.babraham.ac.uk/projects/fastqc/) and, then, low quality regions and adapters were removed using fastp[42]. Cleaned reads were aligned onto the human genome (version hg19) by the ultrafast STAR program[43] providing a list of splice junctions from Gencode[44]. Reads mapping on known human genes were counted using FeatureCounts[45] and differential gene expression was calculated using CuffDiff[40]. Only genes showing p-values < 0.01 were selected for downstream analyses.

Colocalization analysis and statistics

For each immunofluorescence and FISH experiment, two coverslips of cells were probed for the indicated target and 4 to 10 imaging fields were acquired. The number of cells forming EPAC1 condensates was calculated in at least 6 independent experiments and statistical analysis was performed using unpaired t-test. Analysis of co-localization data was performed on selected nuclear regions of interest (ROIs). FISH foci were identified in maximum z-projections and the x and y coordinates were used as reference points to guide the automatic detection of either overlapping or contiguous foci. Manual minimal thresholds were called for the immunofluorescence channels using JaCoP plugin. Overlapping coefficients were then calculated for the FISH foci overlapping EPAC1-YFP foci for at least four images per sample and then averaged. All experiments were repeated at least 3 times with similar results.

Acknowledgments:

Prof. Xiaodong Cheng (University of Texas Health Science Center at Houston) for EPAC1-YFP and EPAC1$^{\Delta 2\text{-}148}$-YFP constructs. We thank Prof. Graziano Martello and Dr. Alessandro Carrer for reading the manuscript. We thank Prof. Luca Scorrano (University of Padua), Dr. Alessandra Dall'Agnese (Whitehead Institute), Prof. Richard A. Young (Whitehead Institute) and Prof. Jin Zhang (UCSD) for helpful discussions and suggestions and the members of the Lefkimmiatis laboratory for helpful discussions. This work was supported by grants from the Foundation "Cassa di Risparmio di Padova

e Rovigo" (CA.RI.PA.RO) (SIGMI), the Italian Ministry of University and Scientific Research (PRIN 2017) and the AIRC foundation for cancer research (project IG2021 ID 26140) to KL. Funding for the RNAseq experiments was obtained from the MIUR - National Research Program (PNR) Flagship InterOmics Project (cod. PB05) to LM.

References:

1. Altarejos, J. Y. & Montminy, M. CREB and the CRTC co-activators: Sensors for hormonal and metabolic signals. *Nat. Rev. Mol. Cell Biol.* **12**, 141–151 (2011).
2. Kvissel, A.-K. *et al.* Involvement of the catalytic subunit of protein kinase A and of HA95 in pre-mRNA splicing. *Exp. Cell Res.* **313**, 2795–809 (2007).
3. Millis, A. J., Forrest, G. A. & Pious, D. A. Cyclic AMP dependent regulation of mitosis in human lymphoid cells. *Exp. Cell Res.* **83**, 335–43 (1974).
4. Sample, V. *et al.* Regulation of nuclear PKA revealed by spatiotemporal manipulation of cyclic AMP. *Nat. Chem. Biol.* **8**, 375–382 (2012).
5. Clister, T., Greenwald, E. C., Baillie, G. S. & Zhang, J. AKAP95 Organizes a Nuclear Microdomain to Control Local cAMP for Regulating Nuclear PKA. *Cell Chem. Biol.* (2019). doi:10.1016/j.chembiol.2019.03.003
6. Robichaux, W. G. & Cheng, X. Intracellular cAMP Sensor EPAC: Physiology, Pathophysiology, and Therapeutics Development. *Physiol. Rev.* **98**, 919–1053 (2018).
7. Di Benedetto, G. *et al.* Compartmentalized Signaling in Aging and Neurodegeneration. *Cells* **10**, (2021).
8. Lefkimmiatis, K. & Zaccolo, M. CAMP signaling in subcellular compartments. *Pharmacol. Ther.* **143**, 295–304 (2014).
9. Harootunian, a T. *et al.* Movement of the free catalytic subunit of cAMP-dependent protein kinase into and out of the nucleus can be explained by diffusion. *Mol. Biol. Cell* **4**, 993–1002 (1993).
10. Dalton, G. D. & Dewey, W. L. Protein kinase inhibitor peptide (PKI): A family of endogenous neuropeptides that modulate neuronal cAMP-dependent protein kinase function. *Neuropeptides* **40**, 23–34 (2006).
11. Saucerman, J. J., Greenwald, E. C. & Polanowska-Grabowska, R. Mechanisms of cyclic AMP compartmentation revealed by computational models. *J. Gen. Physiol.* **143**, 39–48 (2014).
12. Haj Slimane, Z. *et al.* Control of cytoplasmic and nuclear protein kinase A by

phosphodiesterases and phosphatases in cardiac myocytes. *Cardiovasc. Res.* **102**, 97–106 (2014).

13. Burdyga, A. *et al.* Phosphatases control PKA-dependent functional microdomains at the outer mitochondrial membrane. *Proc. Natl. Acad. Sci.* **115**, E6497–E6506 (2018).
14. Grisan, F. *et al.* PKA compartmentalization links cAMP signaling and autophagy. *Cell Death Differ.* (2021). doi:10.1038/S41418-021-00761-8
15. Iannucci, L. F., Di Benedetto, G. & Lefkimmiatis, K. PRKA/PKA signals and autophagy: space matters. *Autophagy* **17**, 1563–1564 (2021).
16. Gerlo, S., Verdood, P., Hooghe-Peters, E. L. & Kooijman, R. Multiple, PKA-dependent and PKA-independent, signals are involved in cAMP-induced PRL expression in the eosinophilic cell line Eol-1. *Cell. Signal.* **17**, 901–909 (2005).
17. Almahariq, M., Mei, F. C. & Cheng, X. The pleiotropic role of exchange protein directly activated by cAMP 1 (EPAC1) in cancer: implications for therapeutic intervention. *Acta Biochim. Biophys. Sin. (Shanghai).* **48**, 75–81 (2016).
18. Fuld, S., Borland, G. & Yarwood, S. J. Elevation of cyclic AMP in Jurkat T-cells provokes distinct transcriptional responses through the protein kinase A (PKA) and exchange protein activated by cyclic AMP (EPAC) pathways. *Exp. Cell Res.* **309**, 161–173 (2005).
19. Huston, E. *et al.* EPAC and PKA allow cAMP dual control over DNA-PK nuclear translocation. *Proc. Natl. Acad. Sci.* **105**, 12791–12796 (2008).
20. Berthouze-Duquesnes, M. *et al.* Specific interactions between Epac1, β-arrestin2 and PDE4D5 regulate β-adrenergic receptor subtype differential effects on cardiac hypertrophic signaling. *Cell. Signal.* **25**, 970–980 (2013).
21. Jansen, S. R. *et al.* Epac1 links prostaglandin E2 to β-catenin-dependent transcription during epithelial-to-mesenchymal transition. *Oncotarget* **7**, 46354–46370 (2016).
22. Gloerich, M. *et al.* The nucleoporin RanBP2 tethers the cAMP effector Epac1 and inhibits its catalytic activity. *J. Cell Biol.* **193**, 1009–1020 (2011).
23. Pereira, L. *et al.* Novel Epac fluorescent ligand reveals distinct Epac1 vs. Epac2 distribution and function in cardiomyocytes. *Proc. Natl. Acad. Sci.* **112**, 3991–3996 (2015).
24. Parnell, E., Smith, B. O. & Yarwood, S. J. The cAMP sensors, EPAC1 and EPAC2, display distinct subcellular distributions despite sharing a common nuclear pore localisation signal. *Cell. Signal.* **27**, 989–96 (2015).
25. Kosugi, S., Hasebe, M., Tomita, M. & Yanagawa, H. Systematic identification of cell cycle-

dependent yeast nucleocytoplasmic shuttling proteins by prediction of composite motifs. *Proc. Natl. Acad. Sci. U. S. A.* **106**, 10171–10176 (2009).

26. Qiao, J., Mei, F. C., Popov, V. L., Vergara, L. A. & Cheng, X. Cell cycle-dependent subcellular localization of exchange factor directly activated by cAMP. *J. Biol. Chem.* **277**, 26581–26586 (2002).

27. Liu, C. *et al.* The Interaction of Epac1 and Ran Promotes Rap1 Activation at the Nuclear Envelope. *Mol. Cell. Biol.* **30**, 3956 (2010).

28. De Rooij, J. *et al.* Epac is a Rap1 guanine-nucleotide-exchange factor directly activated by cyclic AMP. *Nature* **396**, 474–477 (1998).

29. Ponsioen, B. *et al.* Detecting cAMP-induced Epac activation by fluorescence resonance energy transfer: Epac as a novel cAMP indicator. *EMBO Rep.* **5**, 1176–1180 (2004).

30. Sabari, B. R., Dall'Agnese, A. & Young, R. A. Biomolecular Condensates in the Nucleus. *Trends Biochem. Sci.* **45**, 961–977 (2020).

31. Mehta, S. & Zhang, J. Liquid-liquid phase separation drives cellular function and dysfunction in cancer. *Nat. Rev. Cancer* (2022). doi:10.1038/S41568-022-00444-7

32. Alberti, S., Gladfelter, A. & Mittag, T. Considerations and challenges in studying liquid-liquid phase separation and biomolecular condensates. *Cell* **176**, 419 (2019).

33. Zhang, J. Z. *et al.* Phase Separation of a PKA Regulatory Subunit Controls cAMP Compartmentation and Oncogenic Signaling. *Cell* **182**, 1531-1544.e15 (2020).

34. Yoshizawa, T., Nozawa, R.-S., Jia, T. Z., Saio, T. & Mori, E. Biological phase separation: cell biology meets biophysics. *Biophys. Rev.* (2020). doi:10.1007/s12551-020-00680-x

35. Oates, M. E. *et al.* D^2P^2: database of disordered protein predictions. *Nucleic Acids Res.* **41**, (2013).

36. Strom, A. R. & Brangwynne, C. P. The liquid nucleome - phase transitions in the nucleus at a glance. *J. Cell Sci.* **132**, (2019).

37. Mongelard, F. & Bouvet, P. Nucleolin: a multiFACeTed protein. *Trends Cell Biol.* **17**, 80–86 (2007).

38. Nizami, Z., Deryusheva, S. & Gall, J. G. The Cajal body and histone locus body. *Cold Spring Harb. Perspect. Biol.* **2**, (2010).

39. Wang, J. *et al.* Promyelocytic leukemia nuclear bodies associate with transcriptionally active genomic regions. *J. Cell Biol.* **164**, 515–526 (2004).

40. Trapnell, C. *et al.* Differential analysis of gene regulation at transcript resolution with RNA-

seq. *Nat. Biotechnol.* **31**, 46–53 (2013).

41. Duronio, R. J. & Marzluff, W. F. Coordinating cell cycle-regulated histone gene expression through assembly and function of the Histone Locus Body. *RNA Biol.* **14**, 726 (2017).
42. Chen, S., Zhou, Y., Chen, Y. & Gu, J. fastp: an ultra-fast all-in-one FASTQ preprocessor. *Bioinformatics* **34**, i884–i890 (2018).
43. Dobin, A. *et al.* STAR: ultrafast universal RNA-seq aligner. *Bioinformatics* **29**, 15–21 (2013).
44. Frankish, A. *et al.* GENCODE reference annotation for the human and mouse genomes. *Nucleic Acids Res.* **47**, D766–D773 (2019).
45. Liao, Y., Smyth, G. K. & Shi, W. featureCounts: an efficient general purpose program for assigning sequence reads to genomic features. *Bioinformatics* **30**, 923–930 (2014).

Figures and Figure Legends

Figure_1

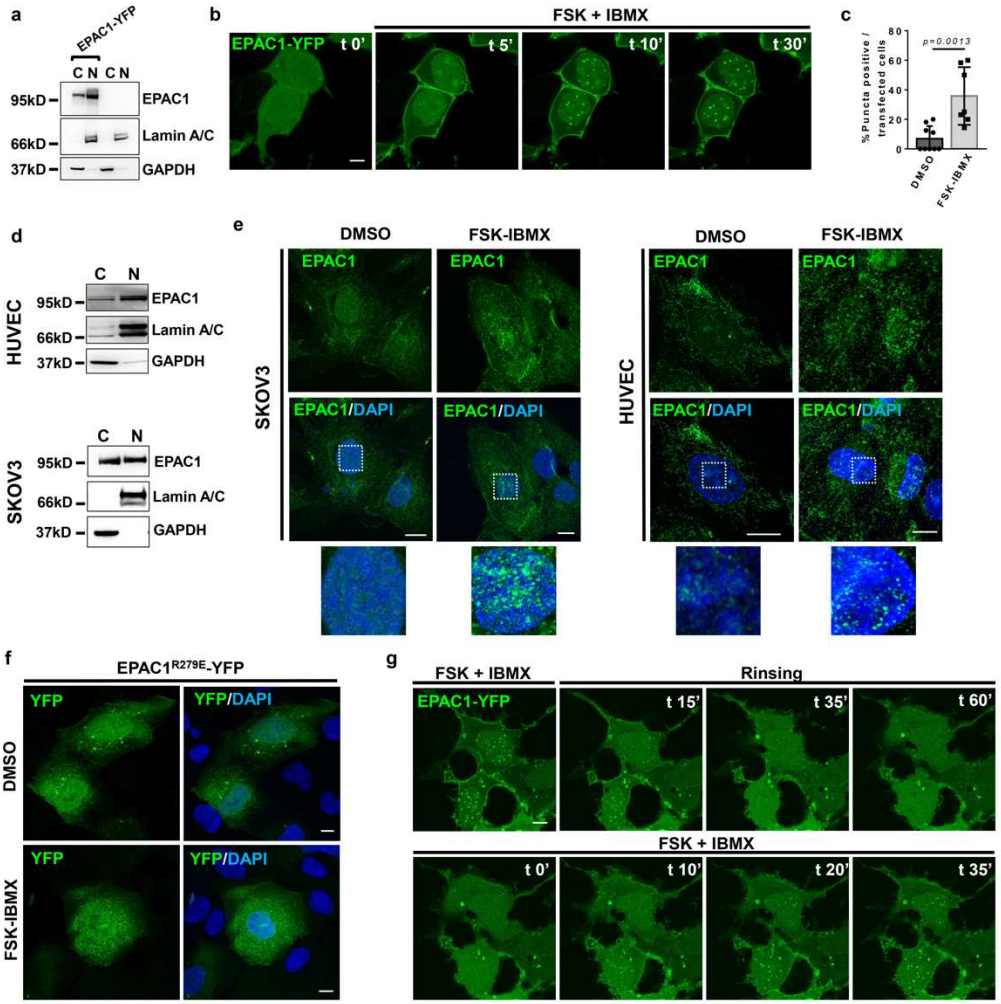

Fig. 1| The nuclear EPAC1 moiety forms reversible oligomers in response to cAMP elevations. a, Western blotting of cytosol and nuclei-enriched fractions of naïve (right lanes) or EPAC1-YFP expressing HEK cells (left lanes). **b**, Live confocal imaging of EPAC1-YFP in HEK cells. In response to cAMP elevating agonists (forskolin (FSK) combined to IBMX) cytosolic EPAC1 moves to plasma membrane while nuclear EPAC1 forms round-shaped structures. Scale bar 5µm **c**, Quantification of EPAC1-YFP expressing HEK cells forming nuclear EPAC1-YFP oligomers (over the total transfected). **d**, Western blotting of cytosol and nuclei-enriched fractions of HUVEC and SKOV3 cells. **e**, Confocal photomicrographs of endogenous EPAC1 distribution in cells (HUVEC, SKOV3) treated with DMSO (control) or forskolin in combination to IBMX (FSK-IBMX) to increase cAMP levels. **f**, Confocal photomicrographs of HEK cells expressing the cAMP-binding deficient mutant EPAC1^{R279E}-YFP. Scale bar 10µm **g**, Live confocal imaging of EPAC1-YFP. Cells were pretreated with FSK-IBMX to induce nuclear EPAC1-YFP oligomerization for 30 minutes. Upon rinsing EPAC1 oligomers dissolve to be formed again in response to subsequent treatment with FSK-IBMX. [FSK] 20µM, [IBMX] 400µM. Scale bar 8µm. Lamin A/C and GAPDH nuclear and cytosolic markers respectively. Nuclei were visualized using DAPI. C: cytosol; N: nucleus. Experiments were repeated at least three times with similar results.

Figure_2

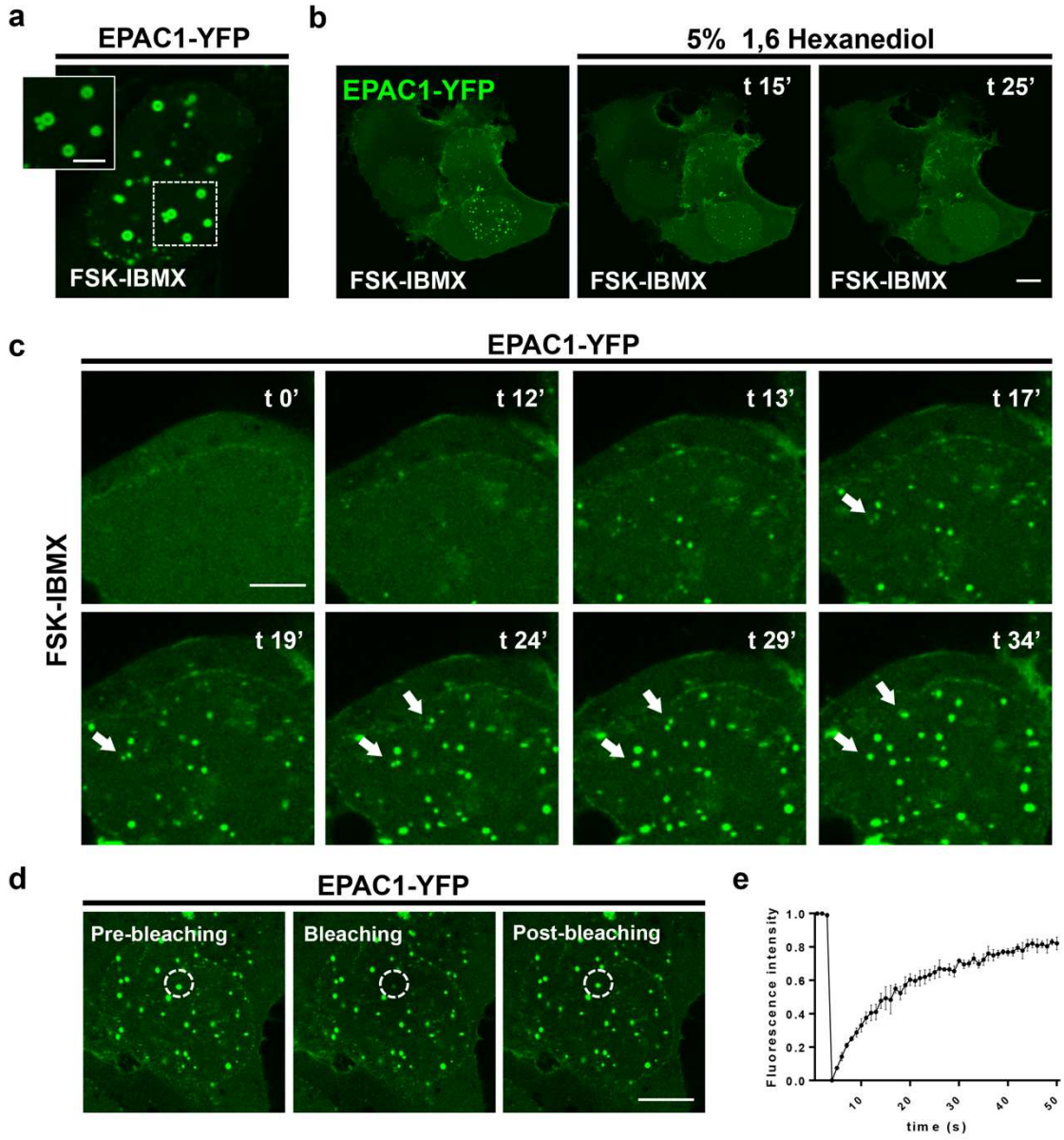

Fig. 2| Nuclear EPAC1 oligomers are biomolecular condensates and form via liquid-liquid phase separation. a, Confocal microphotograph showing the characteristic round hollow shape of EPAC1-YFP condensates after 60 min of FSK-IBMX treatment. Scale bar 10µm (enlargement: 2 µm). **b**, Live confocal imaging of HEK cells expressing EPAC1-YFP. Addition of 5% 1,6-hexaenadiol on top of FSK-IBMX disperses the nuclear EPAC1-YFP condensates. **c**, Live confocal imaging of HEK cells expressing EPAC1-YFP. Treatment with FSK-IBMX triggers the formation of condensates and several fusion events of adjacent condensates are evidenced (arrows). Scale bar 5µm. **d**, Live confocal FRAP experiments (Fluorescence Recovery After Photobleaching). The fluorescence of a single nuclear EPAC1-YFP condensate was targeted with maximal laser power which bleached the fluorescent molecules present in the condensate. Fluorescence rapidly recovered demonstrating the exchange with unbleached molecules from the soluble surrounding. Scale bar 10µm. **e**, Quantification of fluorescence intensity of four independent experiments shows 80% of recovery within 60 seconds from the bleaching event. [FSK] 20µM, [IBMX] 400µM. Unless otherwise stated experiments were repeated at least three times with similar results.

Figure_3

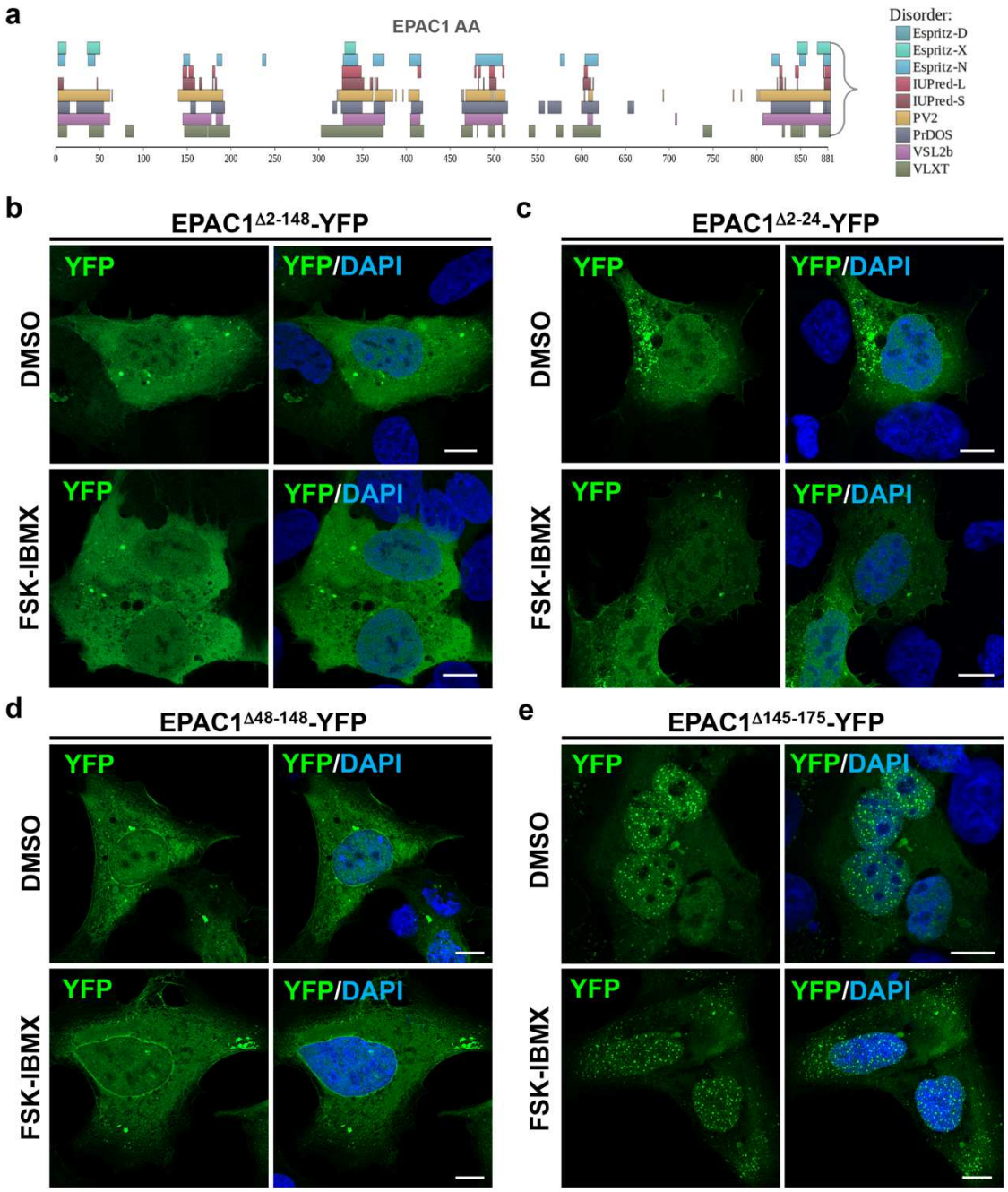

Fig. 3| The amino-terminus of EPAC1 contains Low Complexity Regions necessary for phase transition. a, Schematic map of the intrinsically disordered region distribution within EPAC1 using the bioinformatic algorithm D^2p^2, which takes advantage of several specialized IDR prediction tools (listed on the right). Confocal images of HEK cells expressing the deletion mutant EPAC1$^{\Delta 2\text{-}148}$-YFP (**b**) or EPAC1$^{\Delta 2\text{-}24}$-YFP (**c**) or EPAC1$^{\Delta 48\text{-}148}$-YFP (**d**). All three mutants were unable to undergo phase transition in response to FSK-IBMX treatment. **e**, Confocal images of HEK cells expressing the deletion mutant EPAC1$^{\Delta 145\text{-}175}$-YFP. This construct formed condensates constitutively and independently of the cAMP levels. Nuclei were visualized using DAPI. [FSK] 20µM, [IBMX] 400µM. Scale bar 10µm. Experiments were repeated at least three times with similar results.

Figure_4

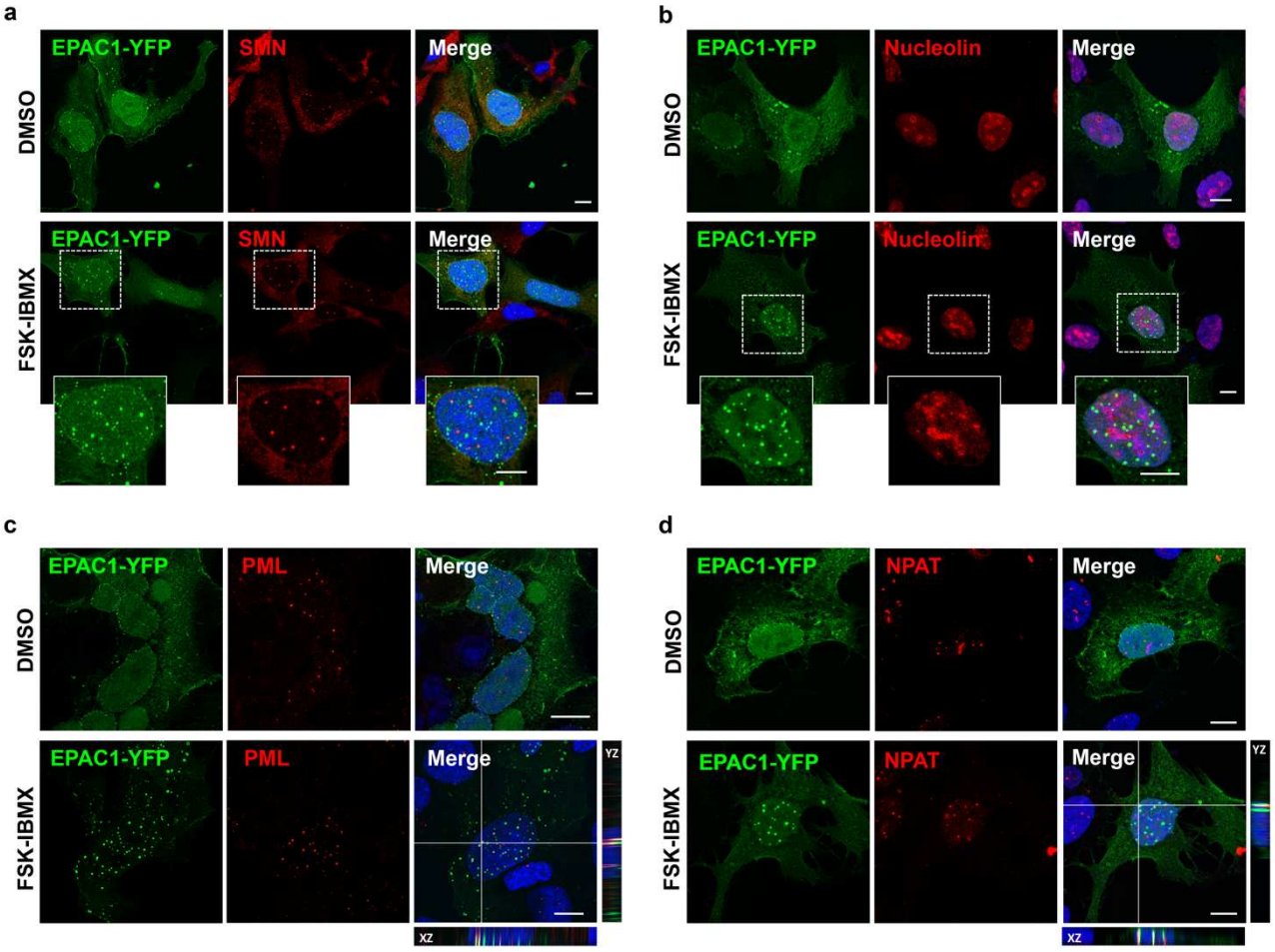

Fig. 4| EPAC1 condensates partially colocalize with PML-nuclear bodies and Histone-Locus Bodies. Confocal photomicrographs of HEK cells expressing EPAC1-YFP and probed for endogenous SMN (survival motor neuron) protein to identify Cajal bodies (**a**) or Nucleolin for identifying the nucleoli (**b**). Neither marker overlapped with EPAC1-YFP. **c**, Confocal images of endogenous PML (red) to map PML-NBs and EPAC1-YFP (green). Several overlapping spots were observed between the two organelles (orthogonal view in last panel). **d**, Confocal images of endogenous NPAT (Nuclear Protein, Ataxia-Telangiectasia Locus) (red) to recognize histone locus bodies (HLBs) and EPAC1-YFP (green). Several points of overlap were observed (orthogonal view in last panel). Nuclei were visualized using DAPI. [FSK] 20µM, [IBMX] 400µM. Scale bar 10µm. Experiments were repeated at least three times with similar results.

Figure_5

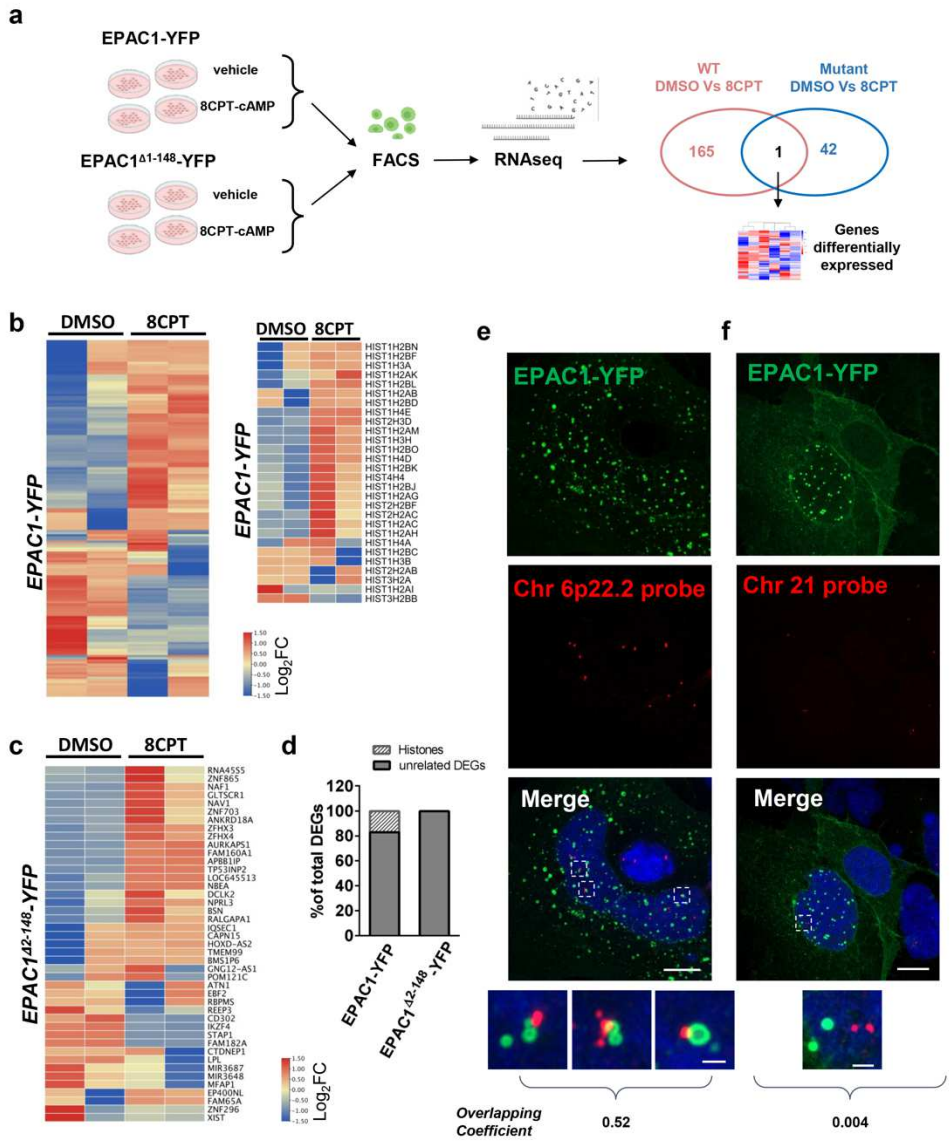

Fig. 5| EPAC1 condensates regulate the transcription of the large Histone cluster 1 on chromosome 6. a, Schematic representation of the experimental design used for the RNAseq experiments. **b**, Heatmap of differentially expressed genes (DEGs) between EPAC1-YFP-expressing HEK cells treated with DMSO or the EPAC1 specific activator 8CPT-cAMP (5µM). Significantly upregulated genes (p<0,01) are represented in red while significantly downregulated are in blue. ***Inset:*** histone genes differentially expressed. **c**, Heatmap of DEGs between EPAC1$^{\Delta 2\text{-}148}$-YFP-expressing HEK cells treated with DMSO or 8CPT-cAMP (5µM). **d**, EPAC1-YFP fluorescence-FISH colocalization experiments in HEK cells treated with FSK-IBMX. The chromosome 6 p22.2 locus was labeled using a custom-made probe (red spots). Significant overlap between the DNA probe and EPAC1-YFP was observed in around 40% of the labeled Chr 6p22.2 locus (overlapping coefficient (0.52) (10 cells)) **e**, EPAC1-YFP fluorescence-FISH experiments in HEK cells treated with FSK-IBMX and probing the unrelated chromosome 21 (21q22.13-q22.2) locus, labeled using a commercial probe (red spots). No overlap between the DNA probe and EPAC1-YFP was observed (overlapping coefficient (0.004) (4 cells)). Nuclei were labeled with DAPI. All experiments were repeated 3 times with similar results. [FSK] 20µM, [IBMX] 400µM. Scale bar 10µm (enlargement 1µm).

Extended data figures

Extended data Figure_1

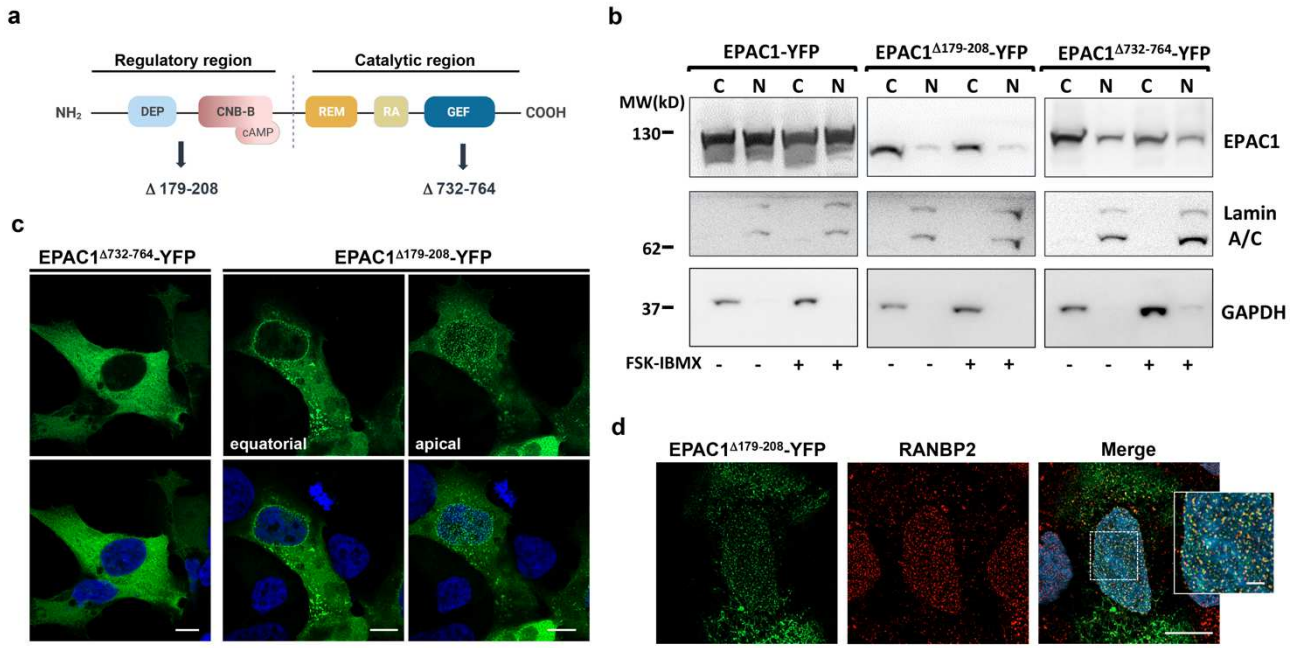

Extended data Fig. 1| Two distinct amino acidic region regulate the entry of EPAC1 in the nucleus. **a**, Schematic representation of putative nuclear localization sequences within EPAC1 identified using the NLS Mapper algorithm. **b**, Western blotting of cytosol and nuclei-enriched fractions of HEK cells EPAC1-YFP, EPAC1$^{\Delta 179\text{-}208}$-YFP and EPAC1$^{\Delta 732\text{-}764}$-YFP. As compared to the WT construct, nuclear localization of both deletion mutants was hindered. Lamin A/C nuclear marker, GAPDH cytosolic marker. **c**, Confocal photomicrographs of EPAC1$^{\Delta 732\text{-}764}$-YFP (left panels) and EPAC1$^{\Delta 179\text{-}208}$-YFP right panels (apical and equatorial views). **d**, Confocal images of cells expressing EPAC1$^{\Delta 179\text{-}208}$-YFP (green) and probed for endogenous RANBP2 (red). Nuclei were labeled using DAPI (blue). C: cytosol; N: nucleus. Experiments were repeated at least three times with similar results. All scale bars 10µm except inset in d (2µm).

Extended data Figure_2

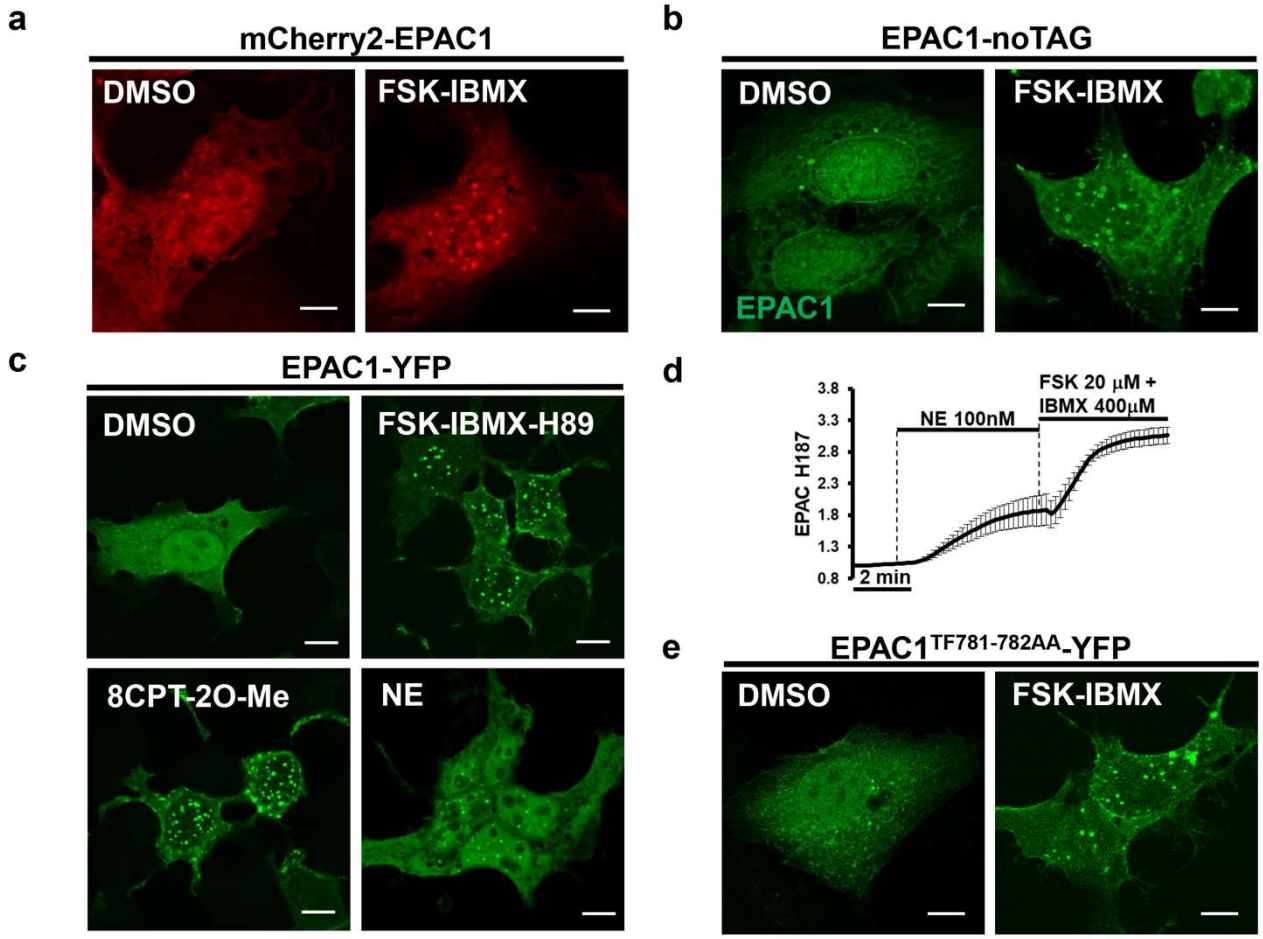

Extended data Fig. 2| EPAC1 oligomerization is independent of PKA and EPAC1 activity. a, Confocal photomicrographs of HEK cells expressing an EPAC1 construct tagged with the monomeric fluorescent protein mCherry2 to its carboxy terminus. **b**, Confocal photomicrographs of HEK cells expressing untagged EPAC1 and probed with a specific anti-EPAC1 antibody. **c**, Confocal photomicrographs of HEK cells expressing EPAC1-YFP and treated with DMSO, FSK-IBMX combined to the PKA inhibitor H89 (30μM), the EPAC1 specific cell permeable cAMP analog 8CPT-cAMP (5μM) or norepinephrine (NE), 100nM. **d**, FRET-based experiment using the cAMP sensor EPAC^{H187} demonstrate that NE treatment induces roughly 50% of the cAMP production induced by FSK-IBMX. **e**, Confocal images of the catalytically dead mutant EPAC1$^{TF781-782AA}$-YFP. Nuclei were stained using DAPI. [FSK] 20μM, [IBMX] 400μM. Scale bar 10μm. Experiments were repeated at least three times with similar results.

Extended data Figure_3

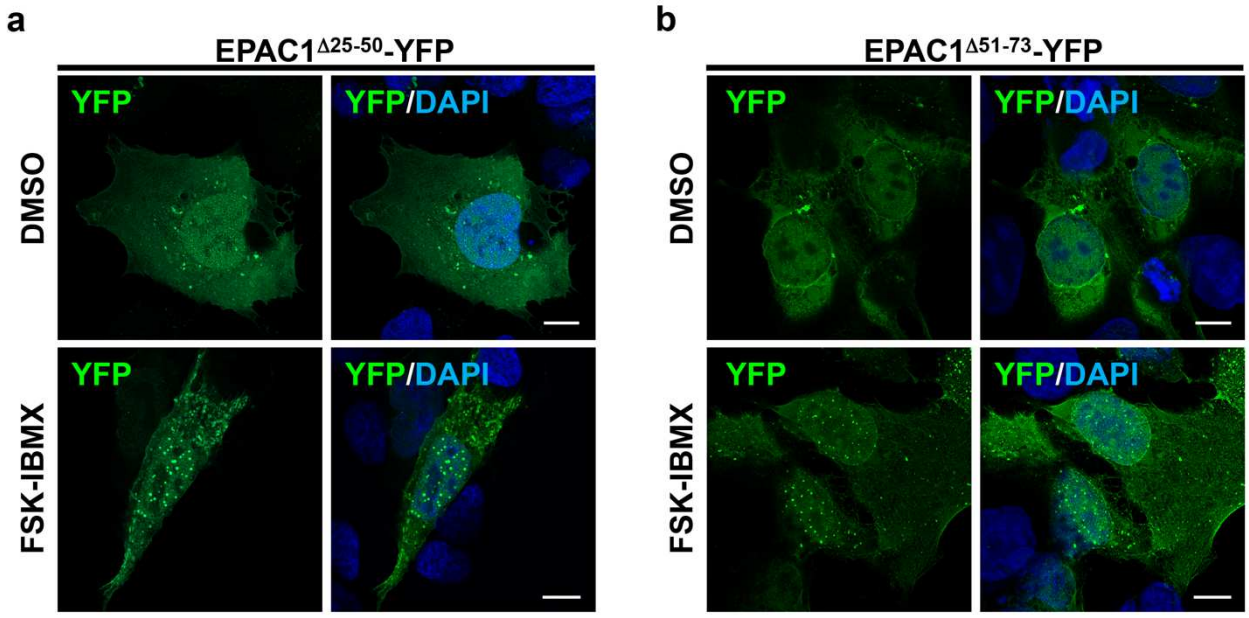

Extended data Fig. 3| Deletion of specific amino acids from the N-terminus of EPAC1 does not affect its ability to phase-separate. Confocal images of HEK cells expressing the deletion mutant EPAC1$^{\Delta 25\text{-}50}$-YFP (**a**) or EPAC1$^{\Delta 51\text{-}73}$-YFP (**b**). Both mutants were able to form condensates in response to cAMP elevations induced by FSK-IBMX. Nuclei were stained using DAPI. [FSK] 20µM, [IBMX] 400µM. Scale bar 10µm. Experiments were repeated at least three times with similar results.

Extended data Figure_4

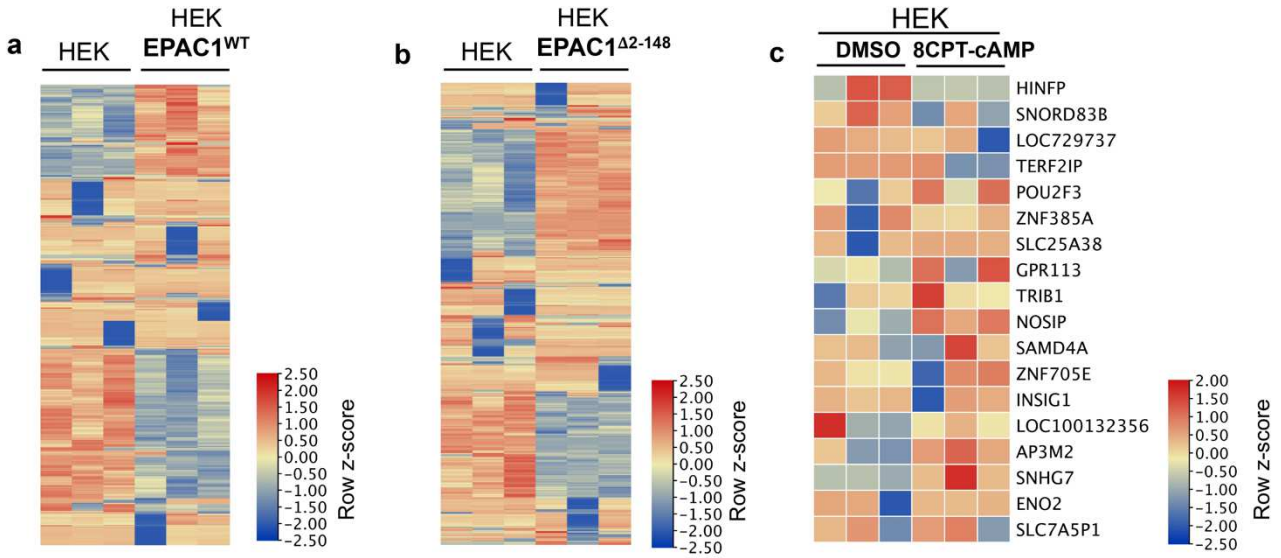

Extended data Fig. 4| Overexpression of EPAC1-YFP or EPAC1$^{\Delta 2\text{-}148}$-YFP changes the transcriptional signatures of EPAC1-deficient HEK cells. Heatmap of gene expression comparing the expression signatures of naïve HEK cells to those of HEK cells expressing EPAC1-YFP (**a**) or EPAC1$^{\Delta 2\text{-}148}$-YFP (**b**). **c**, Heatmap of naïve HEK cells treated with vehicle (DMSO) or the EPAC1-specific cell permeant cAMP analog 8CPT-cAMP (5µM).

Supplementary Files

This is a list of supplementary files associated with this preprint. Click to download.

- reportingsummarynew.pdf
- HEKEPAC1YFPCondensatesmovie1.avi
- HEKEPAC1YFPCondensatesReversemovie2.avi
- EPAC1YFPHexamovie3.avi
- EPAC1YFPfusionmovie4.avi
- EPAC1FRAPmovie5.avi